Elevation resolution enhancement in 3D photoacoustic imaging using FDMAS beamforming

Abdulrhman Alshaya*, Sevan Harput†,David M. J. Cowell*,Thomas Carpenter*, James R. McLaughlan*‡, and Steven Freear*
*Ultrasonics and Instrumentation Group, School of Electronic and Electrical Engineering, University of Leeds, Leeds, LS2 9JT, UK.
†Department of Bioengineering, Imperial College London, London, SW7 2BP, UK.
‡Leeds Institute of Cancer and Pathology, School of Medicine, University of Leeds, Leeds, LS2 9JT, UK.
E-mail: ml11a7a@leeds.ac.uk and S.Freear@leeds.ac.uk

***Abstract*—Photoacoustic imaging is a non-invasive and non-ionizing imaging technique that combines the spectral selectivity of laser excitation with the high resolution of ultrasound imaging. It is possible to identity the vascular structure of the cancerous tissue using this imaging modality. However, elevation and lateral resolution of photoacoustic imaging is usually poor for imaging target. In this study, three dimension filter delay multiply and sum beamforming technique (FDMAS(3D)) is used to improve the resolution and enhance the signal to noise ratio (SNR) of the 3D photoacoustic image that is created by using linear array transducer. This beamforming technique showed improvement in the elevation by 36% when its compared with three dimension delay and sum beamforming technique (DAS(3D)). In addition, it enhanced the SNR by 13 dB compared with DAS (3D).**

I. Introduction

Photoacoustic imaging is used to visualize different structure of the biological tissues based on the wavelength of the absorbed laser pulse [1]. As a result, this type of imaging can be used to measure the oxygen saturation on the blood and detect the early stage of breast cancer [2]. The resolution of the photoacoustic imaging depends on the bandwidth of the ultrasound transducer [3]. This is because the photoacoustic signals that is generated due to the thermoleastic expansion is broadband signals. In addition, this type of imaging is effected by the field of view (FOV) of the ultrasound transducer. To get better viewing for absorbent tissue, three dimension (3D) photoacoustic imaging is used. In the 3D photoacoustic imaging different ultrasound transducers are used such as circular view transducer, matrix transducer, linear array transducer [4]. Linear array transducer have advantages over others types of ultrasound transducers in teams of price, commercial used. In addition, by using linear array transducer, it is easy to combine ultrasound image with photoacoustic image [5]. However, linear array transducer have poor resolution in the elevation direction and suffer from clutter signals.

There are some researchers try to improve the elevation resolution of the photoacoustic image when linear array transducer is used. For instance, Schwarz et.al [6] have applied bi-directional scan by using linear array transducer. Wang et.al [7] have combined coherent factor (CF) with focal line (FL) technique to improve elevation resolution when linear array transducer is used.

In this study, the elevation resolution of the 3D photoacoustic image will be improved when linear array transducer is used by applying Filter delay multiply and sum (FDMAS) beamforming technique in 3D photoacoustic imaging. The FDMAS (3D) beamforming technique will be compared with Delay and Sum (DAS) beamforming technique in terms of spatial resolution and SNR.

II. Method

A. DAS beamforming technique

When a linear array transducer is used in 3D photoacoustic imaging, the RF data for each scanning line is mostly beamformed by using DAS (2D). Then these beamformed data for all scanning lines stack together to form 3D photoacoustic imaging [7]. This 3D photoacoustic image suffers from poor elevation resolution out of the focal point. To reduce the effect of the poor elevation resolution out of the focus point, the received RF data will be beamformed in the lateral then in the elevation directions to generate DAS (3D) beamforming technique [7]. In this beamforming technique, the FOV of each transducer element in the lateral and elevation direction will be taken on account. The equation of DAS (3D) beamforming is shown in Eq.(1) [7]:

$$y_{\mathrm{DAS}} = \sum_{j=1}^{M}\sum_{i=1}^{N} S_{ji}(t) \tag{1}$$

where N is the number of transducer elements, M is the number of scanning lines in the elevation direction and $S_{ji}(t)$ is the delayed RF data that is received by element i in j scanning line.

B. FDMAS beamforming technique

FDMAS is an adoptive beamforming technique that depends on the autocorrelation between delayed RF data [8]. The 2D-FDMAS beamforming technique can be calculated by using Eq.(2) [8]:

$$y_{\mathrm{FDMAS}} = \{\sum_{i=1}^{N-1}\sum_{j=i+1}^{N} sign(S_i(t)S_j(t)).\sqrt{|S_i(t)S_j(t)|}\} * f \tag{2}$$

where $S_i(t)$ and $S_j(t)$ is the delayed RF data for transducer element i and j respectively. The sign and square root operations are used to remove the effect of the multiplication operation on the sign and the unit of the beamformed data. Due to the multiplication operation two frequencies band will be generated. One of these bands is on the baseband. Therefore, bandpass filter (f) will be used to extract the high frequency band.

FDMAS beamforming technique cannot be applied directly in 3D photoacoustic imaging. This is because the FDMAS depends on the autocorrelation operation. To deal with this problem, The FDMAS should be used to beamformed the RF data in the lateral direction and elevation direction separately then combine them. There are two steps to do that. In the first step, the RF data will be beamformed in the lateral direction by using FDMAS. Then the result data will be beamformed again in the elevation direction by using DAS. This step results in improving the lateral resolution and focusing the beamforming data in the elevation direction. In the second step, the RF data will be beamformed in the lateral direction by using DAS. After that these data will be beamformed again in the elevation direction by using FDMAS beamforming technique. This step will lead to enhance the elevation resolution of the photoacoustic image and focus the RF data is the lateral direction. The result of these two steps will be combined before hilbert transform by two techniques. In the first technique the result data for each step will be summed (S-FDMAS(3D)). While in another technique, the result data for each step will be multiplied (M-FDMAS(3D)) with each another as shown in Eq.(3) [6]:

$$y_{\mathrm{M-FDMAS(3D)}} = \sqrt{Y_1 Y_2} \tag{3}$$

where Y_1 is the output data of the first beamforming step and Y_2 is the output data of the second beamforming step. The square root operation is used to save the unit of the data. By combining the result of these two steps, both lateral and elevation resolution will be improved. Fig.1 presents the structure of the FDMAS(3D) beamforming technique.

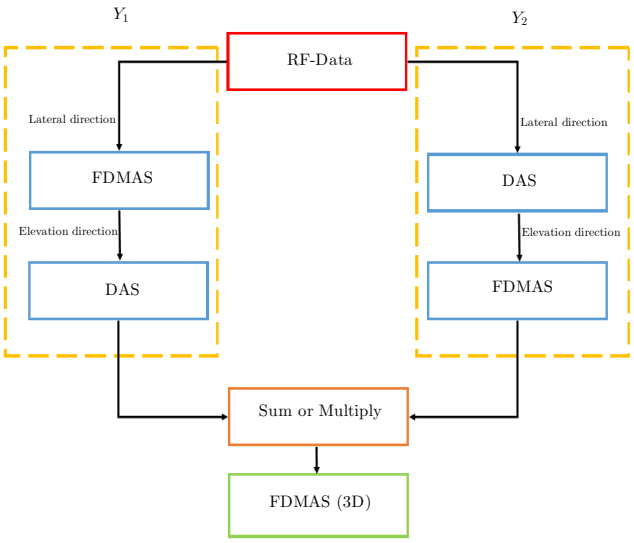

Fig. 1: The structure of FDMAS(3D) beamforming technique.

III. Experiment Setup

A turbid polyacrylamide hydrogel phantom was created with carbon fibre rods as shown in Fig.2. The recipe of this gel phantom is taken from [9], without added ultrasound scattering materials. The diameter of the carbon fibre rods was 2.5λ. Latex beads (1.1μm) were added to achieved 0.3 mm^{-1} optical scattering coefficient [10]. The setup for experiment is shown in Fig.2. The photoacoustic emissions were generated by using tunable Nd:YAG laser. The pulse width and pulse repetition frequency (PRF) of this laser were 7 ns and 10 Hz respectively. The wavelength and the optical energy of the laser were 850 nm and 3.7 mJ respectively. This laser light was applied on the phantom through a optical fibre that its output diameter is 2 mm (NA = 0.22). The generated photoacoustic emissions were recoded by using Ultrasound Array Research Platform II (UARP II) [11], [12] through linear array transducer (Verasonics L11-4v). This transducer consist of 128 elements with a

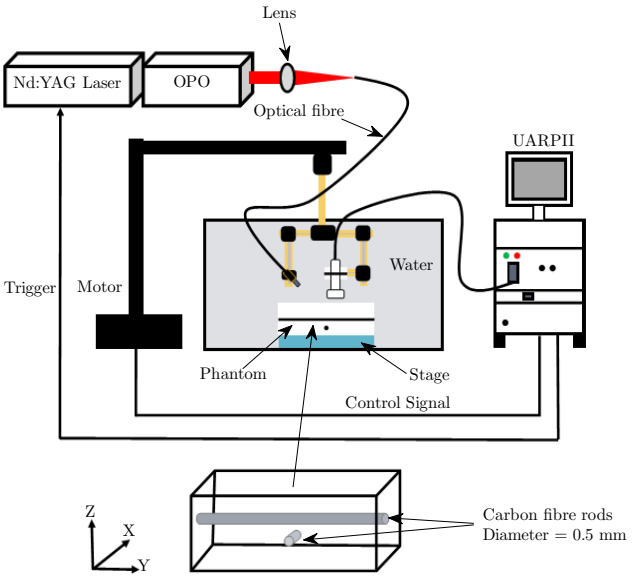

Fig. 2: The experiment setup and the structure of carbon fibre rods phantom.

centre frequency 7.5 MHz and a bandwidth(-6 dB) 90 % . The linear array transducer was moved in the elevation direction by using stepper motor (Zolix, PSA 100-11-X) with step size of 0.1 mm. All transducer elements received the photoacoustic signals simultaneously. These received photoacoustic signals were digitized by 80 MS/s and amplified by 54 dB. These received photoacoustic signals were also averaged over 100 laser pulses before applying the beamforming techniques on them to improve SNR.

IV. RESULT AND DISCUSSION

The FDMAS (3D) beamforming technique was compared with DAS (2D) and DAS(3D) beamforming techniques based on photoacoustic images of carbon fibre rods as shown in Fig.3. These images were reconstructed based on maximum intensity projection (MIP). From these images, it can be noticed that when the photoacoustic image was beamformed based on DAS(2D) (Fig.3 (A)), the background noise of the photoacoustic image is high. This is due to weak of the generated photoacoustic signals and the electrical noise from electrical equipment. In addition, the elevation resolution of this image was poor due to clutter signals. This is because the FOV of the linear array transducer was assumed fixed and narrow in the elevation direction when this image is beamformed.

When the photoacoustic image was beamformed by using DAS(3D) (Fig.3 (B)), the background noise was reduce. This is because that RF data were beamformed in the lateral and elevation directions. In addition, the elevation resolution of the photoacoustic image is mostly improved. This is due to taking the elevation FOV of the transducer on account during the beamforming. This FOV was calculated based on the equations that is used in this reference [13].

However, when FDMAS (3D) beamforming with sum combination (S-FDMAS(3D)) is used, the background noise is significantly decreased as shown in Fig.3 (C). In addition, the elevation resolution is noticeably improved. This improvement will be more enhanced if the FDMAS (3D) beamformer with multiplication combination (M-FDMAS(3D)) is used as shown in Fig.3 (D). The SNR of the photoacoustic image that is beamformed by S-FDMAS(3D) and M-FDMAS(3D) have compared with the SNR of the photoacoustic images that are beamformed by DAS(2D) and DAS(3D) as shwon in Table I. This SNR is defined as a ratio for the maximum intensity of the target signal to the average value of the background noise. The region of the target signal and the background noise are defined as a dashed square region number 1 and number 2 respectively in Fig.3 (D). S-FDMAS (3D) beamformer led to improve the SNR of the photoacoustic image by 19 dB compared with DAS(2D) and by 12 dB compared with DAS(3D). In addition, M-FDMAS (3D) results in improve the SNR by 20 dB and 13 dB compared with DAS(2D) and DAS(3D) respectively. Fig.4 shows 3D visualisation for the carbon fibre rods for DAS(2D), DAS(3D), S-FDMAS(3D) and M-FDMAS (3D) beamforming techniques (The surfaces are extracted with an isosurface value of -30 dB). From this figure, when the DAS(2D) and DAS(3D) beamformers were used, the shape of the carbon fibre rod that is along the elevation direction is hard to define as shown in Fig.4(A) and Fig.4(B). This results of the noise and clutter signals. This is unlike the shape of the carbon fibre rods that results of S-FDMAS(3D) beamformer as shown in Fig.4(C). This beamforming technique reduced the noise and clutter signals. However, when M-FDMAS(3D) beamforming is used, the correlated signal between the two part of the FDMAS(3D) will be emphasize as shown in Fig.4(D).

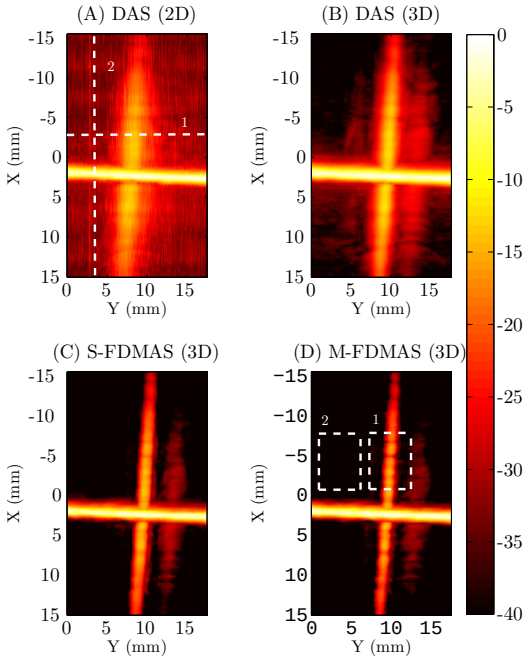

Fig. 3: The photoacosutic images for carbon fibre rods (A) based on DAS(2D) , (B) DAS(3D) (C) S-FDMAS(3D) and (D) M-FDMAS(3D) (-40 dB Dynamic range).

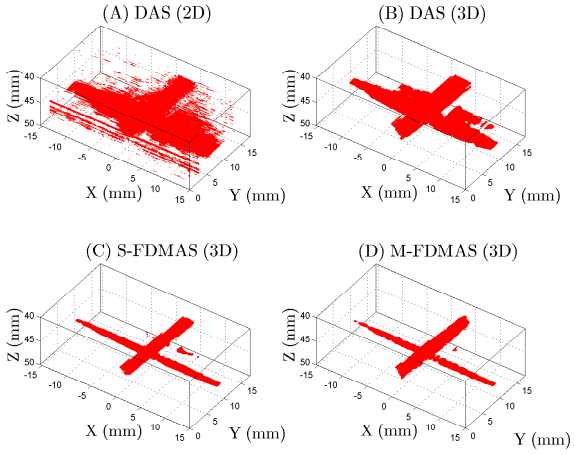

Fig. 4: The 3D photoacoustic image for carbon fibre rods that is beamformed by (A) DAS(2D), (B) DAS(3D), (C) S-FDMAS(3D) and (D) M-FDMAS(3D) (The surfaces are extracted with an isosurface value of -30 dB).

The point spread function in the elevation direction was measured for the carbon fibre rod that is a long elevation direction of the transducer (dashed line number 1 in Fig.3 (A)) as shown in Fig.5 (A). From this figure, it can be noticed that when S-FDMAS(3D) beamforming is used, the full width

at half maximum (FWHM) elevation resolution is improved by 59% and 28% compared with DAS(2D) and DAS(3D) respectively. In addition, when M-FDMAS(3D) is used the elevation resolution is improved by 63% and 36% compared with DAS(2D) and DAS (3D) respectively as shown in Table II. Fig.5 (B) shows the point spread function in the lateral direction for the carbon fibre rod (dashed line number 2 in Fig.3 (A)). S-FDMAS(3D) beamformer leads to slightly improvement in the FWHM lateral resolution (14% and 20% compare with DAS(2D) and DAS(3D) respectively).This is because that the beamformed data that result of DAS is added to the beamformed data that results of FDMAS. This will be effect on the lateral resolution of the image. By using M-FDMAS(3D), the lateral resolution is improved by 8% and 13% compared with DAS(2D) and DAS(3D) respectively as shown in Table II. The sidelobes are extremely reduced when S-FDMAS(3D)and M-FDMAS(3D) are used.

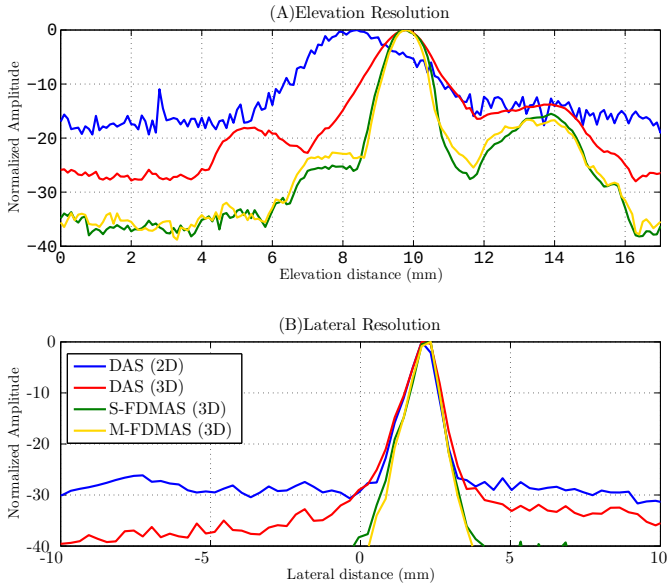

Fig. 5: (A) The point spread function for the carbon fibre rod in the elevation direction and (B) the point spread function for the carbon fibre in the lateral direction.

V. Conclusion

In this study, the FDMAS beamforming technique was applied on 3D photoacoustic imaging when linear array transducer is used. This beamforming technique improved the elevation resolution out of the focus length of linear transducer in the elevation direction. In addition, the correlation operation of this beamformer results in reduce the clutter signals and the background noise of the photoacoustic image. S-FDMAS(3D) and M-FDMAS(3D) showed improvement in the elevation resolution by 28% and 36% respectively compared with DAS(3D). This beamforming technique enhanced the SNR of the photoacoustic image by almost 13 dB compared with DAS(3D). In future work, the effect of this beamforming on complex structure phantom and biological tissue will be studied.

TABLE I: SNR for photoacoustic images.

Beamforming	SNR (dB)
DAS (2D)	16
DAS (3D)	23
S-FDMAS (3D)	35
M-FDMAS (3D)	36

TABLE II: The elevation and lateral resolutions for photoacoustic images.

Beamforming	Elevation Resolution (mm)	Lateral Resolution (mm)
DAS (2D)	3.06	0.75
DAS (3D)	1.74	0.8
S-FDMAS (3D)	1.25	0.64
M-FDMAS (3D)	1.11	0.69

References

[1] V. Ntziachristos, "Going deeper than microscopy: the optical imaging frontier in biology," *Nature methods*, vol. 7, no. 8, pp. 603–614, 2010.

[2] S. Mallidi, K. Watanabe, D. Timerman, D. Schoenfeld, and T. Hasan, "Prediction of tumor recurrence and therapy monitoring using ultrasound-guided photoacoustic imaging," *Theranostics*, vol. 5, no. 3, pp. 289–301, 2015.

[3] S.-L. Chen, S.-W. Huang, T. Ling, S. Ashkenazi, and L. J. Guo, "Polymer microring resonators for high-sensitivity and wideband photoacoustic imaging," *IEEE transactions on ultrasonics, ferroelectrics, and frequency control*, vol. 56, no. 11, pp. 2482–2491, 2009.

[4] J. Xia and L. V. Wang, "Small-animal whole-body photoacoustic tomography: a review," *IEEE Transactions on Biomedical Engineering*, vol. 61, no. 5, pp. 1380–1389, 2014.

[5] C.-W. Wei, T.-M. Nguyen, J. Xia, B. Arnal, E. Y. Wong, I. M. Pelivanov, and M. O'Donnell, "Real-time integrated photoacoustic and ultrasound (paus) imaging system to guide interventional procedures: ex vivo study," *IEEE transactions on ultrasonics, ferroelectrics, and frequency control*, vol. 62, no. 2, pp. 319–328, 2015.

[6] M. Schwarz, A. Buehler, and V. Ntziachristos, "Isotropic high resolution optoacoustic imaging with linear detector arrays in bi-directional scanning," *Journal of biophotonics*, vol. 8, no. 1-2, pp. 60–70, 2015.

[7] D. Wang, Y. Wang, Y. Zhou, J. F. Lovell, and J. Xia, "Coherent-weighted three-dimensional image reconstruction in linear-array-based photoacoustic tomography," *Biomedical optics express*, vol. 7, no. 5, pp. 1957–1965, 2016.

[8] A. Alshaya, S. Harput, A. M. Moubark, D. M. J. Cowell, J. McLaughlan, and S. Freear, "Spatial resolution and contrast enhancement in photoacoustic imaging with filter delay multiply and sum beamforming technique," in *2016 IEEE International Ultrasonics Symposium (IUS)*, Sept 2016, pp. 1–4.

[9] M. J. Choi, S. R. Guntur, K. I. Lee, D. G. Paeng, and A. Coleman, "A tissue mimicking polyacrylamide hydrogel phantom for visualizing thermal lesions generated by high intensity focused ultrasound," *Ultrasound in medicine & biology*, vol. 39, no. 3, pp. 439–448, 2013.

[10] S. Prahl. (2017, Mar.) Mie scattering calculator. [Online]. Available: http://omlc.org/calc/mie_calc.html

[11] P. R. Smith, "Ultrasonic phased array techniques using switched-mode excitation," Ph.D. Thesis, University of Leeds, UK, 2013.

[12] D. M. J. Cowell, P. R. Smith, and S. Freear, "Phase-inversion-based selective harmonic elimination (PI-SHE) in multi-level switched-mode tone- and frequency- modulated excitation," *Ultrasonics, Ferroelectrics and Frequency Control, IEEE Transactions on*, vol. 60, no. 6, pp. 1084–1097, 2013.

[13] S. I. Nikolov and J. A. Jensen, "3d synthetic aperture imaging using a virtual source element in the elevation plane," in *2000 IEEE Ultrasonics Symposium. Proceedings. An International Symposium (Cat. No.00CH37121)*, vol. 2, Oct 2000, pp. 1743–1747 vol.2.